Equation of state for expanded fluid mercury: Variational theory with many-body interaction

Hikaru Kitamura[a)]
Department of Physics, Kyoto University, Sakyo-ku, Kyoto 606-8502, Japan

(Received 17 January 2007; accepted 6 February 2007; published online 6 April 2007)

A variational associating fluid theory is proposed to describe equations of state for expanded fluid mercury. The theory is based on the soft-sphere variational theory, incorporating an *ab initio* diatomic potential and an attractive many-body potential; the latter is evaluated with quatnum chemical methods and expressed as a function of the local atomic coordination number and the nearest-neighbor distance. The resultant equation of state can reproduce the observed gas-liquid coexistence curve with good accuracy, without introducing phenomenological effective pair potentials. Various thermodynamic quantities such as pressure, isochoric thermal pressure coefficient, adiabatic sound velocity, and specific heat are calculated over a wide density-temperature range and compared with available experimental data. © *2007 American Institute of Physics*. [DOI: 10.1063/1.2712443]

I. INTRODUCTION

Expanded fluid metals undergo liquid-gas and metal-nonmetal (M-NM) transitions at high temperatures and high pressures.[1] Mercury, whose gas-liquid critical temperature is the lowest (T_c=1751 K) among all the fluid metals, has so far been most intensively studied; a number of experimental data on thermodynamic, structural, transport, and optical properties are currently available over a wide range of densities and temperatures.[1–4]

Despite of the progress in experimental studies, theoretical models for the equation of state and gas-liquid coexistence curve of mercury have not been established yet, due mainly to the difficulty in describing phase transitions accompanying a drastic change in chemical bonding; the low-density gas phase is dominated by weak van der Waals forces between $6s^2$ closed-shell atoms, whereas the dense liquid phase is characterized by strong metallic cohesion with overlapping $6s$-$6p$ bands. At elevated temperatures near T_c, M-NM transition occurs within the liquid phase at around 9 g/cm^3, which was detected through measurements of the optical excitation gap and the Knight shift.[1,4]

The interplay between the atomic density fluctuation and change in local electronic states brings about interatomic many-body interaction, which is attractive and plays a crucial role in the phase transition.[5] A cooperative attractive interaction would enhance the possibility of temporary cluster formation, i.e., association effect,[6] which significantly affects the optical absorption spectra in dense mercury vapor.[4,7] In principle, atomic motions in the presence of many-body interaction could be simulated with the molecular dynamics method combined with the density-functional electronic-structure calculations,[8] but the construction of phase diagrams and extensive equation-of-state data for fluid mercury has not yet been accomplished through such simulations.

On the other hand, the accurate determination of interatomic interactions in diatomic molecules and small clusters has been achieved, owing to recent progress in *ab initio* quantum-chemical methods[9,10] and spectroscopic studies.[11] It has been revealed that the repulsive part of the potential energy curve of Hg_2 in the ground state is unusually soft as compared to other rare-gas atoms.[11] The origin of the soft repulsion has been ascribed to the admixture of $6s$ and $6p$ states at short ranges, which also contributes to the increment of binding energies in clusters.[12] The outcome of those quantum-chemical analyses would provide a basis for the construction of a theory which facilitates first-principles predictions of fluid phase diagrams.

In this paper, we propose a new equation of state for the expanded fluid mercury which we refer to as the variational associating fluid theory. The theory can treat microscopic interatomic interactions, mesoscopic clustering (association) effect, and macroscopic phase transitions in a coherent fashion, making it possible to predict various thermodynamic quantities without introducing phenomenological state-dependent potentials. The development of such first-principles theory would be indispensable for estimating phase diagrams of other liquid metals whose critical points are not easily accessible through experiments.

In Sec. II, we construct interatomic many-body potentials through quantum-chemical calculations. Free energies are then formulated in Sec. III on the basis of the soft-sphere variational theory. Numerical results on the gas-liquid coexistence curves and various thermodynamic quantities are presented and compared with experimental data in Sec. IV. Concluding remarks and future issues are given in Sec. V.

II. MANY-BODY POTENTIAL

We consider a system composed of N mercury atoms with positional vectors $\{\boldsymbol{r}_i\}$ $(i=1,\ldots,N)$. The total potential energy function $V(\boldsymbol{r}_1,\ldots,\boldsymbol{r}_N)$ can generally be decomposed

[a)]Electronic mail: kitamura@scphys.kyoto-u.ac.jp

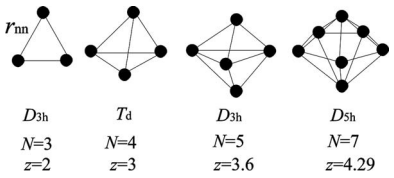

FIG. 1. Cluster geometries adopted in the DIM calculations.

into a pairwise summation of suitably chosen binary potentials and the remaining many-body contribution, that is,

$$V(\boldsymbol{r}_1,\cdots,\boldsymbol{r}_N)=\frac{1}{2}\sum_{\substack{i,j=1\\(i\neq j)}}^{N} V_{\mathrm{dimer}}(|\boldsymbol{r}_i-\boldsymbol{r}_j|)+V_{\mathrm{mb}}(\boldsymbol{r}_1,\cdots,\boldsymbol{r}_N). \quad (1)$$

Specifically, we take $V_{\mathrm{dimer}}(r)$ as a diatomic potential energy curve of Hg_2 in the ground state correlating to $Hg(6^1S)+Hg(6^1S)$ asymptote.[9,11] We adopt the analytic formula by Schwerdtfeger *et al.*[9] based on spin-orbit corrected scalar relativistic coupled cluster calculations using large uncontracted $(11s10p9d4f3g2h)$ basis set (cc-ULB+SO scheme), which reads

$$V_{\mathrm{dimer}}(r)=\lambda_E\frac{e^2}{a_{\mathrm{B}}}\sum_{j=3}^{9}\frac{a_{2j}}{(\lambda_r r/a_{\mathrm{B}})^{2j}}, \quad (2)$$

with $\lambda_E=1.11$, $\lambda_r=1.0143$, $a_6=-1.123\,860\times10^2$, $a_8=-1.095\,406\times10^5$, $a_{10}=1.138\,508\times10^7$, $a_{12}=-4.533\,23\times10^8$, $a_{14}=9.225\,373\times10^9$, $a_{16}=-9.403\,784\times10^{10}$, and $a_{18}=3.801\,021\times10^{11}$. This potential takes on a minimum value of $V_{\mathrm{dimer}}(r)=-0.043$ eV at $r=7.06a_B$, with a_B denoting the Bohr radius.

The basic idea of this work is to evaluate the many-body potential $V_{\mathrm{mb}}(\boldsymbol{r}_1,\ldots,\boldsymbol{r}_N)$ explicitly for particular geometries of clusters and crystalline solids, and to express $V_{\mathrm{mb}}(\boldsymbol{r}_1,\ldots,\boldsymbol{r}_N)/N$ as a function of z (mean coordination number) and r_{nn} (nearest-neighbor distance); these are the two relevant parameters controlling the M-NM transition.[13] For this purpose, we have carried out spin-orbit diatomics-in-molecules (DIM) calculations[12] to evaluate $V_{\mathrm{mb}}(z,r_{\mathrm{nn}})/N$ for small Hg_N clusters with the geometries illustrated in Fig. 1: Hg_3 (D_{3h}), Hg_4 (T_d), Hg_5 (D_{3h}), and Hg_7 (D_{5h}). These geometries may be characterized by $z=2$, 3, 3.60, and 4.29, respectively. We have assumed breathing motions so that the distance r_{nn} of all the nearest-neighbor bonds within a cluster has been changed simultaneously. Numerical calculations have thereby been performed in the range of $5.3\leqslant r_{\mathrm{nn}}/a_B\leqslant6.5$. In this range, mercury clusters remain nonmetallic, with a finite energy gap between the ground and first-excited energy levels.[12]

We have likewise evaluated $V_{\mathrm{mb}}(z,r_{\mathrm{nn}})/N$ for face-centered cubic (fcc) $(z=12)$ and body-centered cubic (bcc) $(z=8)$ structures of bulk solid. These crystalline structures are considered to be metallic, judging from the overlap of 6 *s* and 6*p* bands in the density of states calculated by Mattheiss and Warren Jr.[14] We thus regard the system as a mixture of ions with net charge number $Z=2$ and conduction electrons with number densitiy $n_e=$Zn. The accurate evaluation of the cohesive energies for solid mercury requires careful treatment of the relativistic effect,[15] electrons in the 5*d* band,[15]

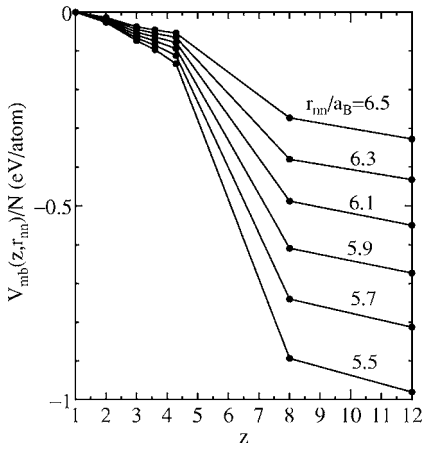

FIG. 2. Many-body potential per atom for various values of r_{nn}. The dots represent the computed data; the solid curves indicate their linear interpolations.

and electron correlation.[16] Simple nearly free electron treatment with local pseudopotentials is not applicable to liquid mercury, but Chekmarev *et al.*[17] showed that addition of empirical corrections leads to considerable improvement of the theory so that reliable predictions of liquid structures and cohesive energies can be achieved at the ambient condition. By following their approach, the cohesive energy per atom may be expressed in a following form:

$$\frac{V}{N}=\frac{1}{2}\sum_{i\geqslant1}N_i\Phi_{\mathrm{eff}}(s_i r_{\mathrm{nn}})+\frac{U_0(n)}{N}, \quad (3)$$

where $\Phi_{\mathrm{eff}}(r)$ describes the density-dependent effective pair potential between ions and $U_0(n)$ is the energy independent of the ionic structure. Expressions for $\Phi_{\mathrm{eff}}(r)$ and $U_0(n)$ are presented in the Appendix. The summation in Eq. (3) describes the interaction of a reference ion with surrounding N_i ions in the *i*th nearest-neighbor shell located at a distance $s_i r_{\mathrm{nn}}$ away from the reference ion. The parameter values for fcc lattice $(z=12)$ are $s_1=1$, $s_2=\sqrt{2}$, $N_1=12$, $N_2=6$, and $n=\sqrt{2}/r_{\mathrm{nn}}$;[3] for bcc lattice $(z=8)$, $s_1=1$, $s_2=2/\sqrt{3}$, $N_1=8$, $N_2=6$, and $n=3\sqrt{3}/4r_{\mathrm{nn}}$.[3] The summation has been truncated at $i=2$, and the contributions from more distant neighbors $(i\geqslant3)$ have safely been neglected. By subtracting the diatomic contribution from Eq. (3), we obtain

$$\frac{V_{\mathrm{mb}}(z,r_{\mathrm{nn}})}{N}=\frac{V}{N}-\frac{1}{2}\sum_{i\geqslant1}N_i V_{\mathrm{dimer}}(s_i r_{\mathrm{nn}}). \quad (4)$$

Numerical values of $V_{\mathrm{mb}}(z,r_{\mathrm{nn}})/N$ so computed are displayed in Fig. 2. We find that the many-body interaction is attractive $(V_{\mathrm{mb}}<0)$ and its magnitude increases as r_{nn} decreases and/or z increases. The microscopic origin of the attraction is attributed to the admixture of excited 6*p* state onto the ground 6*s* state in the electronic wave functions when many atoms aggregate instantaneously.[12] We observe that the magnitude of $V_{\mathrm{mb}}(z,r_{\mathrm{nn}})/N$ is remarkably large in the metallic regime $z\geqslant8$, which means that the short-range repulsive core of the effective interatomic potential in the metallic state is considerably smaller than that in the isolated dimer or small nonmetallic clusters. Such distinctly different behavior of the cohesive energies in the metallic and nonme-

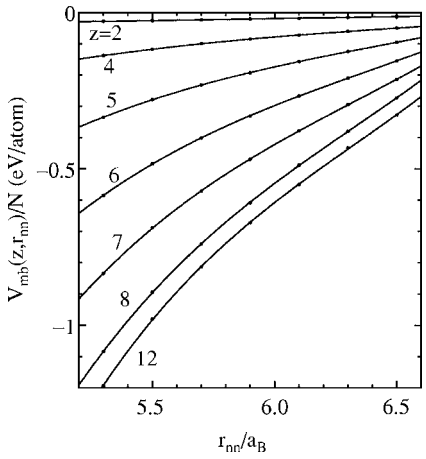

FIG. 3. Many-body potential per atom for various values of z.

tallic states has also been observed in Hg_N clusters, as indicated by Haberland *et al.*:[18] their experimental data exhibit a crossover from nonmetallic to metallic branch in the range $N \approx 15-100$, which may correspond to $z \approx 7-9$ if the cluster geometry is icosahedral and $z \approx 5-8$ if it is tetrahedral.[19] We have no convincing theoretical data for $V_{mb}(z,r_{nn})/N$ in the intermediate-z range where M-NM transition occurs. In this work, we have linearly interpolated the data at $z=4.29$ and $z=8$ as shown by the solid curves in Fig. 2. Though this is a crude treatment of the M-NM transition, we shall see later that the overall feature of the resultant gas-liquid coexistence curve is consistent with experimental observations. The accurate determination of $V_{mb}(z,r_{nn})/N$ for the entire range of z is deferred to a future study. For each z $(z=1,2,\ldots,12)$, we have thus expressed $V_{mb}(z,r_{nn})/N$ as a smooth function of r_{nn}, as exhibited in Fig. 3.

III. EQUATION OF STATE

In this section, we formulate the equation of state for fluid mercury by extending the conventional fluid variational theory of simple fluids[20,21] to the cases of nonsimple fluids.[5] In so doing, the attractive many-body potentials shown in Fig. 3 are taken into consideration. Unlike typical associating fluids such as water,[22] the directional dependence of intermolecular interactions may play a minor role in the case of fluid mercury, because both the van der Waals interactions in the gas phase and metallic bonding in the liquid phase are essentially isotropic. Accordingly, we expect that either a hard-sphere or soft-sphere fluid would serve as an appropriate reference system to mimic the interatomic correlation in fluid mercury.

Ross[21] proposed an approximate soft-sphere variational theory, where correlation functions for the soft-sphere fluid are replaced by those for the hard-sphere fluid, and the soft-core effect is incorporated through an additional empirical correction term in the free energy. We adopt his theory and take the inverse sixth power potential as a reference,[23] with the recognition that the repulsive part of $V_{dimer}(r)$ is rather soft due to the induction effect and approximately proportional[11] to $1/r^{6.2}$. Thus, we write the free energy per atom $f \equiv F/Nk_BT$ as[5]

$$f(n,T;\sigma) = f_{id} - s_{HS}^{ex} + \frac{n}{2k_BT}\int_{\sigma}^{\infty} dr 4\pi r^2 V_{dimer}(r) g_{HS}(r) + \left\langle \frac{V_{mb}(z,r_{nn})}{Nk_BT} \right\rangle_{HS} + f_6. \tag{5}$$

Here,

$$f_{id} = \ln\left[\left(\frac{2\pi\hbar^2}{Mk_BT}\right)^{3/2} n\right] - 1 \tag{6}$$

represents the ideal-gas free energy with $M=3.331 \times 10^{-22}$ g denoting the mass of a Hg atom. The quantities with subscript "HS" are evaluated for the hard-sphere fluid with core diameter σ. The excess entropy is evaluated in the Carnahan-Stirling approximation,[20]

$$s_{HS}^{ex} = -\eta\frac{4-3\eta}{(1-\eta)^2}, \tag{7}$$

with $\eta = \pi n\sigma^3/6$ designating the packing fraction. The last term on the right-hand side of Eq. (5),

$$f_6 = -0.932\,71\eta - 0.495\,05\eta^2 - 2.129\,24\eta^3 + 0.500\,30\eta^4, \tag{8}$$

represents the soft-sphere correction obtained by Young and Rogers.[23] The radial distribution function $g_{HS}(r)$ for the hard-sphere fluid is available in parametrized form by Trokhymchuk *et al.*[24]

The coordination number z of an atom in the fluid may be defined as the number of nearest-neighbor atoms contained within a sphere of suitably chosen volume $v(=4\pi r_{max}^3/3)$ encompassing that atom. The instantaneous value of z differs from atom to atom due to structural disorder. In light of the observations in Figs. 2 and 3, we expect that an atom with larger z and/or smaller r_{nn} may experience a stronger attractive force than that with smaller z and/or larger r_{nn}. Accordingly, we take a statistical average of the quantity $V_{mb}(z,r_{nn})/N$ over all possible realizations of z and r_{nn}. Strictly speaking, the average should be taken for the reference *soft-sphere* system, but since it is difficult to get probability distribution functions of z and r_{nn} for soft-sphere fluids we replace them by the hard-sphere counterparts for simplicity. We also treat z and r_{nn} as statistically independent variables, neglecting their mutual correlations. We thus evaluate the term $\langle\cdots\rangle_{HS}$ in Eq. (5) as

$$\left\langle \frac{V_{mb}(z,r_{nn})}{Nk_BT} \right\rangle_{HS} = \sum_{z=1}^{z_{max}} p_{HS}(z) \frac{\int_{\sigma}^{r_{max}} dr_{nn} H_{HS}(r_{nn}) V_{mb}(z,r_{nn})/Nk_BT}{\int_{\sigma}^{r_{max}} dr_{nn} H_{HS}(r_{nn})}. \tag{9}$$

Here, $p_{HS}(z)$ is the distribution function of z for the hard-sphere fluid. Through simple geometrical considerations within the excluded-volume approximation,[7] we arrive at an expression as follows:

$$p_{\mathrm{HS}}(z) = \frac{p_{\mathrm{HS}}(0)}{z!} \frac{(nv-\eta)(nv-2\eta)\cdots(nv-z\eta)}{(1-\eta)^z}$$

$$\text{for } 1 \leqslant z \leqslant z_{\max}, \tag{10}$$

and $p_{\mathrm{HS}}(0)$ is determined from the normalization $\sum_{z=0}^{z_{\max}} p_{\mathrm{HS}}(z)=1$. In this work, we take the maximum value of z as $z_{\max}=12$ (corresponding to the fcc lattice), and v is chosen as $v=(z_{\max}+1)\pi\sigma^3/6$, leading to $r_{\max}=(z_{\max}+1)^{1/3}\sigma/2 = 1.176\sigma$. In this case, we can prove that $p_{\mathrm{HS}}(0)=(1-\eta)^{z_{\max}}$, and average coordination number is given by

$$\langle z \rangle = \sum_{z=0}^{z_{\max}} z p_{\mathrm{HS}}(z) = z_{\max}\eta, \tag{11}$$

which is proportional to the packing fraction.

The distribution function $H_{\mathrm{HS}}(r_{\mathrm{nn}})$ represents the probability of finding a nearest-neighbor particle at distance r_{nn} from the reference particle. The properties of this function were discussed in detail by Torquato.[25] He obtained an analytic expression for $H_{\mathrm{HS}}(r_{\mathrm{nn}})$ in terms of a dimensionless distance $x \equiv r_{\mathrm{nn}}/\sigma$ as

$$\sigma H_{\mathrm{nn}}(r_{\mathrm{nn}}) = 24\eta(a_0 x^2 + a_1 x + a_2)\exp\{-\eta[8a_0(x^3-1) + 12a_1(x^2-1) + 24a_2(x-1)]\}, \tag{12}$$

with

$$a_0 = 1 + 4\eta g(\sigma), \quad a_1 = \frac{3\eta - 4}{2(1-\eta)} + 2(1-3\eta)g(\sigma),$$

$$a_2 = \frac{2-\eta}{2(1-\eta)} + (2\eta - 1)g(\sigma), \quad g(\sigma) = \frac{1-\eta/2}{(1-\eta)^3}.$$

We note that $H_{\mathrm{HS}}(r_{\mathrm{nn}})$ is a decreasing function of r_{nn} with a peak at $r_{\mathrm{nn}}=\sigma$; the peak becomes sharper as η increases. Our treatment of cooperative interaction represented by Eq. (9) is analogous to the associating fluid model of liquid water by Truskett *et al.*,[22] except for the anisotropic interaction in the latter.

For given n and T, the total free energy $f(n,T,\sigma)$ of Eq. (5) is minimized with respect to the variational parameter σ as $\partial f(n,T,\sigma)/\partial\sigma|_{n,T}=0$. The pressure P, entropy S, internal energy U, and Gibbs free energy G are then calculated in a standard way as $p \equiv P/nk_{\mathrm{B}}T = n(\partial f/\partial n)_T$, $s \equiv S/Nk_{\mathrm{B}} = -[\partial(fT)/\partial T]_n$, $u \equiv U/Nk_{\mathrm{B}}T = f+s$, and $G/Nk_{\mathrm{B}}T = f+p$, respectively; the derivatives in these formulas should be evaluated under the constraint that f be minimized with respect to σ. We remark that both Eqs. (10) and (12) depend on n so that their density derivatives also contribute to the pressure.

IV. NUMERICAL RESULTS

A. Gas-liquid coexistence curves

At sufficiently low temperatures, the derivative $(\partial P/\partial n)_T$ can take on a negative value, indicating the onset of the first-order gas-liquid transition. The saturation densities in the gas and liquid phases, n_{gas} and n_{liq}, are obtained in accordance with the conditions of two-phase equilibrium: $P(n_{\mathrm{gas}},T)=P(n_{\mathrm{liq}},T)$ and $G(n_{\mathrm{gas}},T)=G(n_{\mathrm{liq}},T)$. The gas-liquid coexistence curves so obtained are displayed in Fig. 4

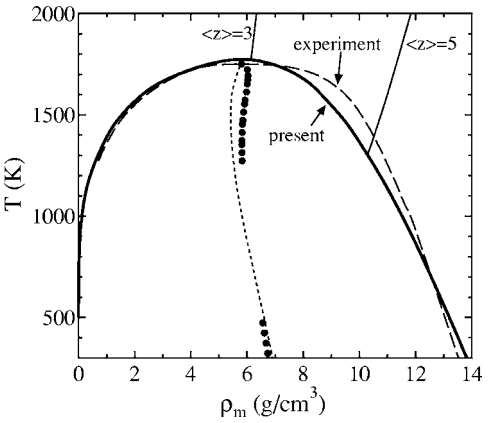

FIG. 4. Gas-liquid coexistence curve on the mass density-temperature plane. The thick solid curve corresponds to the present result; the dashed curve represents the experimental data (Refs. 1 and 3). The mean density ρ_{d} in this work is plotted by the dotted curve; the corresponding experimental data (Refs. 1 and 26) are shown by dots. The thin solid curves depict the contours of constant mean coordination numbers.

(ρ_m-T diagram; $\rho_{\mathrm{m}} \equiv$ Mn) and in Fig. 5 (T-P diagram). It can be seen that our coexistence curves reproduce the experimental data[1,3,26] reasonably well. The critical density, temperature, and pressure are predicted to be $\rho_c=5.82$ g/cm^3, $T_c=1774$ K, and $P_c=1.97$ kbars, which are in good agreement with the corresponding experimental values,[1] $\rho_c(\mathrm{exp})=5.8$ g/cm^3, $T_c(\mathrm{exp})=1751$ K, and $P_c(\mathrm{exp})=1.67$ kbars. At the melting point ($T=234$ K and $P=1$ bar), our theory yields $\rho_{\mathrm{liq}}=\mathrm{Mn}_{\mathrm{liq}}=14.02$ g/cm^3, $S/Nk_{\mathrm{B}}=6.0$, and $U/N=-0.056$ Ry/atom, which compare with the corresponding experimental values:[27] $\rho_{\mathrm{liq}}(\mathrm{exp})=13.65$ g/cm^3, $S(\mathrm{exp})/Nk_{\mathrm{B}}=8.3$, and $U(\mathrm{exp})/N=-0.034$ Ry/atom.

In Fig. 4, we also plot the average of gas and liquid densities $\rho_d = M(n_{\mathrm{gas}}+n_{\mathrm{liq}})/2$. Experimental data[1,26] reveal that $d\rho_d/dT<0$ for sufficiently low temperatures and in the vicinity of the critical point, whereas $d\rho_d/dT>0$ in the range of $T \approx 1400$–1700 K. It is remarkable that the present theory likewise predicts the behavior $d\rho_d/dT>0$ above 1500 K. Ross and Hensel[28] invoked a modified two-state van der Waals model and pointed out that the positive slope of

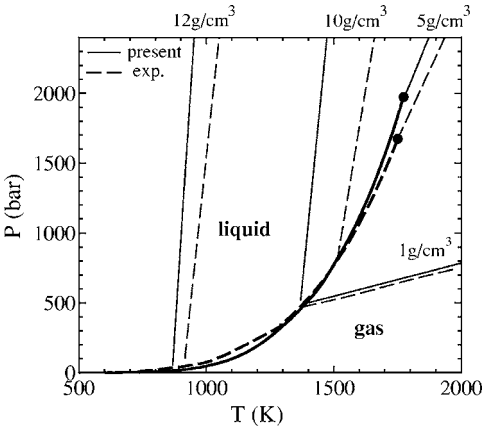

FIG. 5. Gas-liquid coexistence curve on the temperature-pressure plane. The thick solid curve indicates the present result; the thick dashed curve refers to the experimental data (Refs. 1 and 3). The dots represent the corresponding critical points. Thin solid curves indicate isochores at respective densities, compared with experimental data (Refs. 1 and 3) (thin dashed curves).

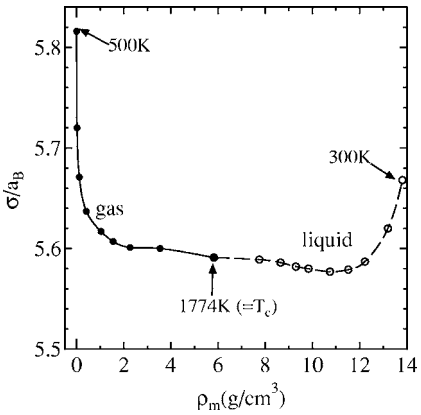

FIG. 6. Optimized values of σ along the coexistence curve. The solid curve with filled circles correspond to the gas phase; the dashed curve with open circles correspond to the liquid phase.

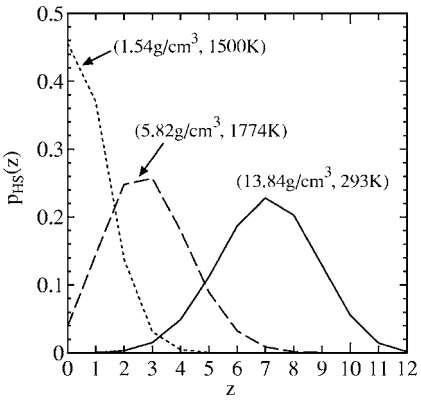

FIG. 7. Distributions of coordination number in the reference hard-sphere fluid.

$d\rho_d/dT$, which is absent in simple rare-gas fluids, is intimately related to the M-NM transition in the liquid phase. We suppose that the strong cohesive force associated with metallization tends to increase the values of n_{liq} in that range.

The gas-liquid coexistence curve is determined through a delicate balance between the free energies in the two phases, and hence it is sensitive to the adopted theoretical model. When fluid mercury is treated as a partially ionized nonideal plasma, the resultant coexistence curve on the ρ_m-T plane becomes too sharp, and the values of n_{liq} are underestimated especially in the M-NM transition range.[29,30] Plasma theories assume that the delocalized electrons extend uniformly over the entire space. Such assumption may not be appropriate in expanded fluid metals: Spatial distributions of electronic wave functions may be governed by the local atomic arrangement, as pointed out by Chacón *et al.*[31] in their tight-binding models of fluid alkali metals. The present model significantly improves our previous plasma-theoretical treatment,[30] but it should be noted in Fig. 4 that our coexistence curve still exhibits small deviation from the experimental data in the M-NM transition range at around 9 $\mathrm{g/cm^3}$. We shall come to this point later in Sec. IV C.

B. Structures

The present theory cannot describe atomic structures of the real system, but qualitative arguments on the structures may be possible through the correlation functions of the reference hard-sphere fluid with optimized core diameters. We see in Fig. 6 that the optimized value of σ along the coexistence curve remains virtually constant ($\sigma/a_B \approx 5.58-5.60$) over a wide density range $\rho_m = 2-12$ $\mathrm{g/cm^3}$. It is notable that this value is close to the observed first peak position of the radial-distribution function, $5.67a_B$, which is likewise almost unchanged within the liquid phase as revealed by the x-ray diffraction experiments.[2] By substituting the optimized σ into Eq. (11), we find that the average coordination number is proportional to the density as $\langle z \rangle \approx 0.49\rho_m$ ($\mathrm{g/cm^3}$) along the coexistence curve (Fig. 7). These features corroborate the picture of inhomogeneous expansion.[2,32]

In Fig. 7, the distribution function $p_{\mathrm{HS}}(z)$ is illustrated for three different points on the coexistence curve. In the low-density gas phase, the distribution has a sharp peak at $z=0$, indicating that the many-body interaction does not contribute appreciably to the equation of state. As the density increases, the position of the peak shifts toward large-z side and the peak height becomes lower, in qualitative agreement with the results of the reverse Monte Carlo simulation by Arai and McGreevy.[32] At the critical point, the three- and four-body interactions ($z=2$ and 3) are predicted to be dominant, but the fluctuation is so large that the atoms having larger z also contribute to the cohesive energy. At the normal liquid density at 293 K, the peak is located at $z=7$ and hence the significant part of the distribution is contained in the metallic domain.

The contours of $\langle z \rangle = 3$ and 5 obtained from Eq. (11) are superposed on the phase diagram in Fig. 4. We find that $\langle z \rangle$ depends not only on ρ_m but also on T. This is because the radius r_{max} of the first coordination region depends on the optimum core diameter σ and the latter becomes small as T increases.

C. Thermodynamic quantities

Isochores at ρ_m ($\mathrm{g/cm^3}$) = 1, 5, 10, and 12 are plotted and compared with experimental data by Götzlaff[3] (taken from Ref. 1) in Fig. 5. The present theory shows fairly good agreement with experiments at the lowest and highest densities, but tends to overestimate the pressure in the M-NM transition regime (10 $\mathrm{g/cm^3}$). Pressure-density relations at constant temperatures (1723 and 1813 K) are likewise presented in Fig. 8. We find that the agreement between theory and experiment is good below the critical density, whereas our equation of state turns out too stiff in the liquid phase at around 9 $\mathrm{g/cm^3}$.

We have also computed isochoric thermal pressure coefficient $\gamma_v \equiv (\partial P/\partial T)_n$, along the coexistence curve. As manifested in Fig. 9, the present theory agrees fairly well with the experimental results at low and high densities, but theoretical values are too large at intermediate densities of 9–12 $\mathrm{g/cm^3}$, suggesting that the effective interatomic interaction is estimated to be too repulsive in this range.

The specific heats at constant volume (C_v) and constant pressure (C_p) are evaluated respectively as

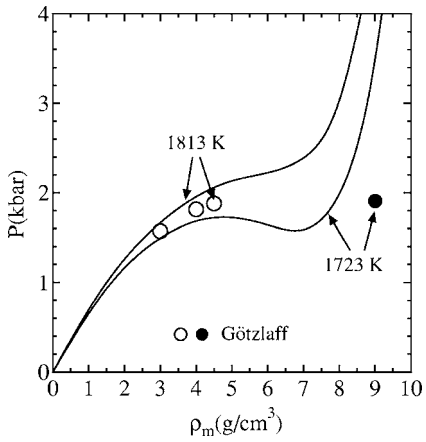

FIG. 8. Pressure-density curve at constant temperatures. The black and white circles refer to the experimental data (Refs. 2 and 3).

$$\frac{C_v}{N} = \left(\frac{\partial}{\partial T}\left(\frac{U}{N}\right)\right)_n, \quad \frac{C_p}{N} = \frac{C_v}{N} + \frac{T}{n^2}\frac{\gamma_v^2}{(\partial P/\partial n)_T}. \tag{13}$$

In Fig. 10, the predictions of Eq. (13) at $P=2$ kbars are illustrated and compared with direct calorimetric measurements by Levin and Schmutzler.[33] It turns out that the overall agreement between theory and experiment is fairly good for C_v. Levin and Schmutzler found a shallow minimum of C_v at $\rho_m=9.2$ g/cm^3, and they speculated that it might be caused by the omission of the electronic contribution to the heat capacity as the transition from metallic to nonmetallic phase occurs.[33] Such minimum has not been detected in this work, however; C_v decreases monotonically with decreasing density and eventually approaches 3/2 corresponding to the ideal-gas value of the monoatomic gas. The value of C_p obtained from Eq. (13) is somewhat larger than the measured value at the highest density ($\rho_m=12.4$ g/cm^3), but both theoretical and experimental data exhibit strong critical divergence of C_p as the density decreases and approaches ρ_c. In the gas phase, C_p decreases rapidly toward the ideal-gas value of 5/2.

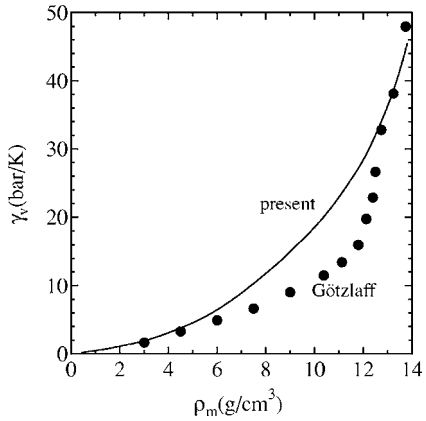

FIG. 9. Isochoric thermal pressure coefficient along the gas-liquid coexistence curve. The solid curve represent the present result; dots depict the experimental data (Refs. 1 and 3).

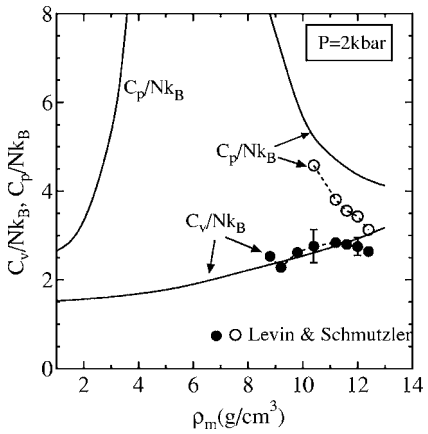

FIG. 10. Specific heats C_v and C_p evaluated with Eq. (13) at $P=2$ kbars (solid curves). The black and white circles with an error bar depict experimental data by Levin and Schmutzler (Ref. 33).

The adiabatic sound velocity is defined and calculated as

$$c_s = \sqrt{\left(\frac{\partial P}{\partial \rho_m}\right)_S} = \sqrt{\frac{1}{M}\left\{\left(\frac{\partial P}{\partial n}\right)_T + \frac{T}{n^2}\frac{\gamma_v^2}{C_v/N}\right\}}. \tag{14}$$

In Fig. 11, theoretical values of c_s at $P=2$ kbars are presented and compared with the experimental measurements by Kohno and Yao.[34] In the low-density gas phase, Eq. (14) reduces to the ideal-gas expression $c_s=\sqrt{5k_BT/3M}$. At densities higher than about 4 g/cm^3, our theory tends to overestimate the sound velocity, though a qualitative trend of the experimental data is reproduced. The deviation between theory and experiment is enlarged particularly in the M-NM transition range around $\rho_m=9$ g/cm^3. The experimental curve exhibits an inflection at $\rho_m=9$ g/cm^3, whereas our theoretical curve shows a rather smooth density dependence. The inflection was reproduced through the molecular dynamics simulation by Munejiri *et al.*,[35] who deduced an effective interatomic pair potential from measured static structure factors and claimed that change in the repulsive part of the potential causes the inflection.

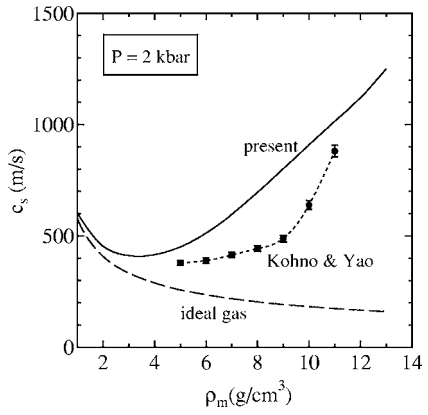

FIG. 11. Adiabatic sound velocities at $P=2$ kbars. The solid curve represents the prediction of Eq. (14); the dots with error bars are experimental data by Kohno and Yao (Ref. 34); the dashed curve is the result for monatomic ideal gas.

V. CONCLUDING REMARKS

Previous theoretical analyses of thermodynamic properties in the expanded fluid mercury were limited to empirical modifications of the van der Waals equations[1,28] or computer simulations using density- or temperature-dependent effective pair potentials adjusted to reproduce existing experimental data.[35–37] These methods would not be useful if experimental data are not available in advance. In contrast, the variational associating fluid theory developed here is the first to predict thermodynamic quantities of fluid mercury by using quantum-chemical interatomic interactions as input, without resorting to empirical state-dependent pair potentials. A salient feature of the present scheme lies in its *cross-hierarchical* nature, bridging the gap between macroscopic thermodynamics and microscopic interatomic interactions by taking additional account of the mesoscopic association effects. Our theory is also advantageous from the practical point of view, in a sense that various thermodynamic quantities can be obtained over a wide density-temperature range without massive computations. Though the theory has been applied exclusively to mercury in this work, the formalism is quite general and would be applicable to other fluids after suitable modifications.

We have stressed the importance of the attractive many-body interaction among atoms, which becomes strong as the local coordination number (z) increases and the nearest-neighbor distance (r_{nn}) decreases. The statistical average of the potential has been carried out by taking into account fluctuations of z and r_{nn} in the reference hard-sphere fluids. As exposed in Figs. 2 and 3, the many-body potential in mercury is relatively weak in the nonmetallic, small-z regime, while it becomes substantially strong in the metallic, large-z regime. As the density increases, the atomic coordination increases and a strong cohesive force is produced, which plays a dominant role in the gas-liquid transition. Along the coexistence curve, we have found that the average coordination number is nearly proportional to the density while the optimized core diameter (and hence the distance of the closest approach) is virtually constant, supporting the inhomogeneous expansion mechanism. We have also computed such thermodynamic quantities as isochoric thermal pressure coefficient, sound velocity, and specific heats, which show reasonable agreement with experimental data.

In the M-NM transition region at around 9 g/cm^3, however, our equation of state systematically overestimates the pressure, and fails to account for the abrupt change of the isochoric thermal pressure coefficient and sound velocity detected by experiments. To elucidate possible origins of those discrepancies, we mention two issues to be investigated in the future: First, we should improve the data in Figs. 2 and 3 in the intermediate-z regime by performing accurate electronic-structure calculations and see how the present equation of state is modified. The second problem is the possibility of *heterophase fluctuation* in the M-NM transition, characterized by inhomogeneous mixing of metallic and nonmetallic domains.[30,38] The possibility of an inhomogeneous structure was suggested through recent experimental observations, such as anomalous sound attenuation[34] and fast sound.[39] The present theory may overlook the emergence of a heterophase fluctuation, because the structural information is included solely in the hard-sphere reference system characterized by only one parameter σ. On the other hand, the previous mesoscopic simulation by the author[30] was based on the coarse-grained theory, where the interatomic many-body interaction was not treated correctly. Further development of the theory is needed so as to treat thermodynamics, structures, and electronic states on an equal footing.

ACKNOWLEDGMENTS

The author thanks Dr. F. Hensel, Dr. R.M. More, Dr. R. Redmer, Dr. M. Yao, and Dr. H. Yoneda for pertinent discussions. This work was supported in part through Grant-in-Aid for Scientific Research provided by the Japanese Ministry of Education, Science, Sports and Culture.

APPENDIX: COHESIVE ENERGIES OF METALLIC SOLIDS

In the conventional local pseudopotential theory of nearly free-electron metals,[20] the pair potential between ions is calculated as

$$\Phi(r) = \frac{(Ze)^2}{r} + \frac{1}{2\pi^2}\int_0^\infty dk k^2 \Phi_{BS}(k)\frac{\sin(kr)}{kr}, \tag{A1}$$

where

$$\Phi_{BS}(k) = \frac{4\pi(Ze)^2}{k^2}\left[\frac{1}{\varepsilon_e(k)} - 1\right]\left|\frac{V^p(k)}{4\pi Ze^2/k^2}\right|^2. \tag{A2}$$

Here, $V^p(k)$ refers to the Fourier transform of the bare electron-ion pseudopotential $V^p(r)$, and $\varepsilon_e(k)$ designates the dielectric function of the homogeneous electron liquid at density n_e, where strong exchange and Coulomb correlations are incorporated through the static local-field correction $G(k)$.[40,41] Chekmarev *et al.*[17] modified Eq. (A1) by adding the repulsive Born-Mayer potential of the form $\Phi_{BM}(r) = A(e^2/a_B)\exp(-Br/a_B)$ to obtain the improved effective ion-ion interaction as

$$\Phi_{eff}(r) = \Phi(r) + \Phi_{BM}(r). \tag{A3}$$

The coefficients A and B are adjusted[17] so that the pair-distribution functions computed with Eq. (A3) agree with experimental data.

The structure-independent energy per ion may be evaluated as

$$\frac{U_0(n)}{N} = \frac{ZF_{eg}}{N_e} + \frac{E_H}{N} - \frac{n}{2}\Phi(k=0) + \frac{E_{BS}^{self}}{N} + I_p + \frac{e^2}{a_B}\left(\frac{C_1}{r_s} + \frac{C_2}{r_s^2}\right). \tag{A4}$$

Here, F_{eg}/N_e denotes the free energy per electron of the homogeneous electron liquid, whose analytic expressions are available in the literature.[40] The Hartree energy is defined as[20]

$$\frac{E_H}{N} = n_e \int d\mathbf{r} \left[V^p(r) + \frac{Ze^2}{r} \right]. \tag{A5}$$

The self-part of the band-structure energy is calculated in accordance with Eq. (A2) as[20]

$$\frac{E_{\mathrm{BS}}^{\mathrm{self}}}{N} = \frac{1}{4\pi^2} \int_0^\infty dk k^2 \Phi_{\mathrm{BS}}(k). \tag{A6}$$

The ionization potential I_p is an energy required to remove valence electrons from an isolated atom. The final term on the right-hand side of Eq. (A4) corresponds to the empirical correction which ensures mechanical stability and a correct value of the cohesive energy.[17] Here, we have introduced the dimensionless electron-density parameter $r_s = a_e/a_B$, with $a_e = (3/4\pi n_e)^{1/3}$ denoting the Wigner-Seitz radius.[40]

When the Ashcroft empty-core pseudopotential[20] with the core radius R_c is adopted for $V^p(r)$, we have $V^p(k) = (-4\pi Ze^2/k^2)\cos(kR_c)$ and $\Phi(k=0) = 4\pi(Ze)^2(D_L^2 + R_c^2)$. Here, D_L represents the long-range screening distance of the electrons defined as $D_L^2 = \lim_{k\to 0}[1/k^2\varepsilon_e(k)] = a_e^2[(\pi\lambda/4r_s) - \lambda^2\gamma_0(r_s)]$, with $\lambda = (4/9\pi)^{1/3}$; $\gamma_0(r_s) = \lim_{k\to 0}[G(k)/(k/k_F)^2]$ is related to the long-wavelength limit of the local-field correction $G(k)$, with $k_F = (3\pi^2 n_e)^{1/3}$ denoting the Fermi wave number.[40] An analytic expression for $G(k)$ was presented by Ichimaru and Utsumi.[40,41]

In applying the above formalism to liquid mercury, we follow Chekmarev *et al.*[17] and adopt $R_c = 0.915a_B$, $A = 200$, and $B = 2$. The sum of the first and second ionization potentials for an isolated Hg atom amounts to $I_p/k_B = 3.388 \times 10^5$ K. In Eq. (A4), we have set $C_1 = -0.197$ and $C_2 = 0.6$ so that the observed cohesive energy of 0.67 eV/atom is reproduced for the fcc lattice ($z = 12$); although the rhombohedral structure is slightly more stable than fcc in the ground state, the linear muffin-tin orbital (LMTO) calculation by Bose[42] showed that the relative difference between the cohesive energies of these two lattice structures is as small as 2%. Our theory predicts the optimum lattice constant of the fcc solid to be $6.07a_B$, in good agreement with the LMTO result,[42] $6.04a_B$.

[1] F. Hensel and W. W. Warren, Jr., *Fluid Metals* (Princeton University Press, Princeton, 1999).
[2] M. Inui, X. Hong, and K. Tamura, Phys. Rev. B **68**, 094108 (2003).
[3] W. Götzlaff, Ph. D. thesis, Phillipps-Universität Marburg, 1988.
[4] M. Yao, Z. Phys. Chem. **185**, S73 (1994).
[5] H. Kitamura, J. Phys.: Condens. Matter **19**, 072102 (2007).
[6] E. A. Müller and K. E. Gubbins, Ind. Eng. Chem. Res. **40**, 2193 (2001).
[7] R. N. Bhatt and T. M. Rice, Phys. Rev. B **20**, 466 (1979).
[8] G. Kresse and J. Hafner, Phys. Rev. B **55**, 7539 (1997).
[9] P. Schwerdtfeger, R. Wesendrup, G. E. Moyano, A. J. Sadlej, J. Grief, and F. Hensel, J. Chem. Phys. **115**, 7401 (2001).
[10] M. Dolg and H.-J. Flad, Mol. Phys. **91**, 815 (1997).
[11] J. Koperski, Phys. Rep. **369**, 177 (2002).
[12] H. Kitamura, Chem. Phys. Lett. **425**, 205 (2006); Chem. Phys. **325**, 207 (2006).
[13] I. N. Yakovin and P. A. Dowben, J. Chem. Phys. **112**, 7622 (2000).
[14] L. F. Mattheiss and W. W. Warren, Jr., Phys. Rev. B **16**, 624 (1977).
[15] P. P. Singh, Phys. Rev. B **49**, 4954 (1994).
[16] B. Paulus and K. Rosciszewski, Chem. Phys. Lett. **394**, 96 (2004).
[17] D. S. Chekmarev, M. Zhao, and S. A. Rice, Phys. Rev. E **59**, 479 (1999).
[18] H. Haberland, H. Kornmeier, H. Langosch, M. Oschwald, and G. Tanner, J. Chem. Soc., Faraday Trans. **86**, 2473 (1990).
[19] H.-G. Fritsche and R. E. Benfield, Z. Phys. D: At., Mol. Clusters **26**, 15 (1993).
[20] N. W. Ashcroft and D. Stroud, Solid State Phys. **33**, 1 (1978); M. Hasegawa and W. H. Young, J. Phys. F: Met. Phys. **11**, 977 (1981).
[21] M. Ross, J. Chem. Phys. **71**, 1567 (1979).
[22] T. M. Truskett, P. G. Debenedetti, S. Sastry, and S. Torquato, J. Chem. Phys. **111**, 2647 (1999).
[23] D. A. Young and F. J. Rogers, J. Chem. Phys. **81**, 2789 (1984).
[24] A. Trokhymchuk, I. Nezbeda, J. Jirsák, and D. Henderson, J. Chem. Phys. **123**, 024501 (2005).
[25] S. Torquato, Phys. Rev. E **51**, 3170 (1995).
[26] N. Mehdipour and A. Boushehri, Int. J. Thermophys. **18**, 1329 (1997).
[27] M. Shimoji, *Liquid Metals* (Academic, London, 1977).
[28] M. Ross and F. Hensel, J. Phys.: Condens. Matter **8**, 1909 (1996).
[29] R. Redmer, Phys. Rep. **282**, 35 (1997).
[30] H. Kitamura, J. Phys.: Condens. Matter **15**, 6427 (2003).
[31] E. Chacón, J. P. Hernandez, and P. Tarazona, Phys. Rev. B **52**, 9330 (1995); E. Chacón, M. Reinaldo-Falagán, P. Tarazona, E. Velasco, and J. P. Hernandez, *ibid.* **71**, 024204 (2005).
[32] T. Arai and R. L. McGreevy, J. Phys.: Condens. Matter **10**, 9221 (1998).
[33] M. Levin, and R. W. Schmutzler, J. Non-Cryst. Solids **61&62**, 83 (1984).
[34] H. Kohno, and M. Yao, J. Phys.: Condens. Matter **11**, 5399 (1999).
[35] S. Munejiri, F. Shimojo, and K. Hoshino, J. Non-Cryst. Solids **250–252**, 144 (1999).
[36] G. Raabe and R. J. Sadus, J. Chem. Phys. **119**, 6691 (2003).
[37] J.-M. Bomont and J.-L. Bretonnet, J. Chem. Phys. **124**, 054504 (2006).
[38] M. H. Cohen and J. Jortner, Phys. Rev. A **10**, 978 (1974).
[39] M. Inui, D. Ishikawa, K. Matsuda, K. Tamura, S. Tsutsui, and A. Q. R. Baron, J. Phys. Chem. Solids **66**, 2223 (2005).
[40] S. Ichimaru, *Statistical Plasma Physics*, Condensed Plasmas Vol. 2 (Addison-Wesley, Reading, MA, 1994), Chap. 3.
[41] S. Ichimaru and K. Utsumi, Phys. Rev. B **24**, 7385 (1981).
[42] S. K. Bose, J. Phys.: Condens. Matter **11**, 4597 (1999).